Thermodynamic Dissociation Constant of the Bisulfate Ion from Raman and Ion Interaction Modeling Studies of Aqueous Sulfuric Acid at Low Temperatures

D. A. Knopf,* B. P. Luo, U. K. Krieger, and Thomas Koop

Institute for Atmospheric and Climate Science, Swiss Federal Institute of Technology, Honggerberg HPP, 8093 Zurich, Switzerland

Received: December 19, 2002; In Final Form: March 27, 2003

The dissociation reaction of the bisulfate ion, $HSO_4^- \rightleftharpoons SO_4^{2-} + H^+$, is investigated in aqueous H_2SO_4 solutions with concentrations of 0.54−15.23 mol kg^{-1} in the temperature range of 180−326 K using Raman spectroscopy. All investigated H_2SO_4 solutions show a continuous increase in the degree of dissociation of HSO_4^- with decreasing temperature, in contrast to predictions from thermodynamic models of aqueous H_2SO_4 solutions. A Pitzer ion interaction model is used to derive a thermodynamically consistent formulation of the thermodynamic dissociation constant of the bisulfate ion, $K_{II}(T)$, that is in agreement with the experimental data. The new formulation of $K_{II}(T)$ is valid from 180 to 473 K. All ion interaction parameters and the corresponding parametrizations of the Pitzer ion interaction model are presented. Calculations with this model reveal significant differences in ion activity coefficients, water activities, water vapor pressure, and HCl solubilities, when compared to existing thermodynamic models of H_2SO_4/H_2O solutions, in particular at lower temperatures.

Introduction

Aqueous sulfuric acid (H_2SO_4) is one of the most important mineral acids in chemical industries.[1] Because of this, its thermodynamic properties such as partial pressures as well as osmotic and activity coefficients were intensively studied over the past decades.[2−5] In the atmosphere, sulfuric acid affects many properties of ambient aerosols. Stratospheric background aerosols consist of highly concentrated aqueous sulfuric acid droplets.[6,7] Tropospheric aerosols can contain mixtures of various inorganic and organic species, but H_2SO_4 is often a major component.[8] Furthermore, the solubility of volatile gases such as HCl and NH_3 in liquid aerosols depends on the concentration of dissolved H^+-ions,[9,10] which, in turn, depends on the degree of dissociation of H_2SO_4. The dissociation of H_2SO_4 is a two-step process:

$$H_2SO_4 \rightleftharpoons HSO_4^- + H^+ \quad \text{(I)}$$

$$HSO_4^- \rightleftharpoons SO_4^{2-} + H^+ \quad \text{(II)}$$

It has been shown that the dissociation of H_2SO_4 is essentially complete for concentrations up to 40 mol kg^{-1} at temperatures between 273 and 323 K.[11] These measurements further suggest that full dissociation occurs also at lower temperatures at these concentrations. On the other hand, the dissociation of the bisulfate ion, HSO_4^-, depends strongly on temperature.[11−15] The thermodynamic dissociation constant of the HSO_4^--ion, $K_{II}(T)$, is defined by the activities of the particular ions (see Appendix for a full derivation of $K_{II}(T)$):

$$K_{II}(T) = \frac{a_{H^+}(T)a_{SO_4^{2-}}(T)}{a_{HSO_4^-}(T)} \quad (1)$$

$$= \frac{m_{H^+}(T)m_{SO_4^{2-}}(T)}{m_{HSO_4^-}(T)m^\dagger}\frac{\gamma_{H^+}(T)\gamma_{SO_4^{2-}}(T)}{\gamma_{HSO_4^-}(T)} \quad (2)$$

$$= Q(T)\cdot\gamma(T) \quad (3)$$

where a_i, m_i, and γ_i denote the activity, molality, and activity coefficient of ion i ($i = H^+, SO_4^{2-}, HSO_4^-$) in equilibrium, $m^\dagger$ is by definition 1 mol kg^{-1}, and $Q(T)$ and $\gamma(T)$ are the molal dissociation quotient and activity coefficient product, respectively.

Knowledge of $K_{II}(T)$ is a prerequisite for the description of the thermodynamic properties of a multicomponent system containing H_2SO_4, such as the $NH_3/H_2SO_4/H_2O$ system at atmospheric temperatures (≈180−300 K). However, there are only a few experimental studies of the properties of aqueous H_2SO_4 at low temperatures.[15−18] Therefore, thermodynamic solution models are employed to predict ion activity coefficients and ion concentrations in aqueous solutions at low temperatures in a consistent way. One widely used model of this kind is the aerosol inorganics model (AIM),[19] which is based on the Pitzer ion interaction approach.[20] Since low-temperature data on the dissociation of sulfuric acid are not available, the formulation of the thermodynamic dissociation constant $K_{II}(T)$ that has been implemented in the AIM model[19,21] is the one taken from Dickson et al.,[14] who derived $K_{II}(T)$ from measurements in the temperature range of 298−523 K.

* To whom correspondence should be addressed. E-mail: Daniel.Knopf@iac.umnw.ethz.ch.

10.1021/jp027775+ CCC: $25.00
Published on Web 04/26/2003

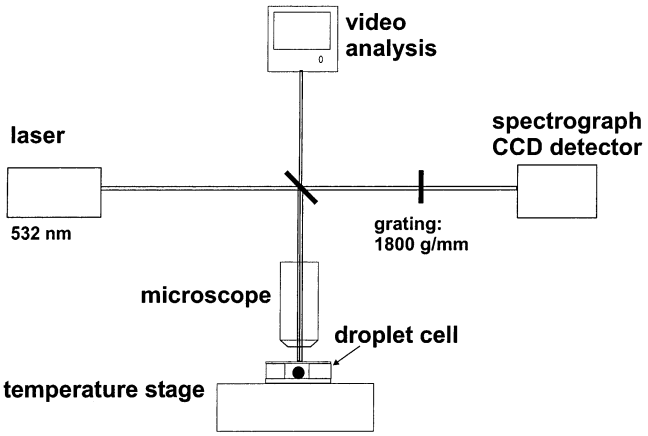

Figure 1. Sketch of the experimental setup.

One way to experimentally investigate the dissociation of the bisulfate ion is Raman spectroscopy. Raman data of aqueous H_2SO_4 solutions in the temperature range of 278−328 K[11] are available, but the only existing Raman study at temperatures below 273 K focused on H_2SO_4/H_2O solutions in the glassy state and investigated the dissociation of the bisulfate ion in more detail only for a solution 4.37 mol kg^{-1} in concentration to 233 K.[15]

In this paper we present new experimental data on the degree of dissociation of the bisulfate ion in sulfuric acid solutions derived from Raman spectroscopic measurements at concentrations of 0.54−15.23 mol kg^{-1} and temperatures of 180−326 K. We use a Pitzer ion interaction model[20] to derive a thermodynamically consistent formulation of $K_{II}(T)$ which is in agreement with the experimental data. The ion activity coefficients, γ_{H^+}, $\gamma_{SO_4^{2-}}$, and $\gamma^2_{H^+}\cdot\gamma_{SO_4^{2-}}$, and water activity, a_w, for selected H_2SO_4 solutions are calculated using the new formulation of $K_{II}(T)$. These results are compared to values derived by the AIM model of Clegg et al.[19]

Experimental Section

Figure 1 shows the experimental setup. Raman spectra of aqueous droplets are obtained using a confocal Raman microscope (Jobin Yvon, model Labram) operated with a Nd:YAG laser at a wavelength of 532 nm and a power of 25−100 mW for illumination. The backscattered light is passed onto a grating (1800 mm^{-1}) and focused on the CCD detector of the spectrograph. The resulting spectral resolution is about 2−4 cm^{-1} within the observed range of 500−4000 cm^{-1}. A homemade temperature stage is attached to the microscope table. The temperature of the stage can be varied between 180 and 326 K. The temperature was measured using a resistance temperature sensor (Pt 100) whose linear resistance/temperature response was confirmed by measuring the melting points of heptane, octane, decane, dodecane, and water. Phase changes (i.e. freezing or melting) are observed visually with the microscope part of the setup.

Table 1 shows the composition of the investigated solutions of H_2SO_4/H_2O and $(NH_4)_2SO_4/H_2O$. The H_2SO_4 solutions were prepared from stock solutions which were titrated against 1 M NaOH. The $(NH_4)_2SO_4$ solutions were prepared from solid[4] $(NH_4)_2SO_4$ and Millipore water (resistivity ≥ 18.2 MΩ·cm). In addition, the solutions were filtered through a 0.2 μm pore size membrane. The volume of the droplets varied between 0.5 and 10 μL (diameters of about 0.1−0.26 cm). The droplets were deposited with a micropipet on a silanized (hydrophobic) quartz plate inside a laminar flow clean bench. Either an O-ring or a Teflon washer treated with high-vacuum grease served as a spacer for a second quartz plate, which sealed the droplets against ambient air. Afterward the droplet cell was placed on the temperature stage.

TABLE 1: Composition and Volume of the Investigated Aqueous Droplets

composition		
H_2SO_4 (mol kg^{-1})	$(NH_4)_2SO_4$ (mol kg^{-1})	volume ($\times 10^{-3}$ cm^3)
0.54	0	10
1.13	0	0.5
2.55	0	0.5
4.37	0	0.5
6.79	0	0.5
9.84	0	10
15.23	0	10
0	0.99	0.5
0	1.95	0.5
0	3.17	0.5
0	3.88	1
0	5.35	1

A typical experiment started by taking a Raman spectrum at room temperature. Subsequently, the droplet was either cooled or heated in temperature steps of 5−10 K (at a rate of 10 K min^{-1}) and a new Raman spectrum was taken at each temperature.

To exclude any possible bias in the temperature and composition of the droplet due to the energy transfer from the laser light, a sensitivity study was performed. At a fixed temperature of 298 K, Raman spectra were recorded, in which a droplet was exposed to different illumination times and laser intensities. Figure 2 shows 12 Raman spectra of a H_2SO_4/H_2O droplet 10 μL in volume with a concentration of 4.37 mol kg^{-1}. Six of the 12 Raman spectra were taken with a laser power of 100 mW and varying laser excitation times between 1 s and 1 h. The other 6 Raman spectra were recorded with a laser power of 25 mW and varying illumination times from 1 s to 2 h. The Raman spectra are indistinguishable from each other, showing that the energy transfer from the laser into the droplets has no significant influence on the droplet composition or temperature, which would have been seen as a change in the vibration band ratio $\nu_1(SO_4^{2-})/\nu_1(HSO_4^-)$ (see below). The influence of the laser light on droplet temperature was also checked by measuring melting temperatures of aqueous nitric acid droplets while they were excited by the laser.[22] The experimentally obtained melting temperatures were in agreement with literature data[23] within 1 K, which also indicates that no significant change in composition occurred.

Results and Discussion

To determine the ion activity product, $\gamma(T)$, in an aqueous H_2SO_4 solution, measured values of $Q(T)$ and data on $K_{II}(T)$ are required. In the following, we present the analysis of the experimental data and derive a new formulation of $K_{II}(T)$ using a Pitzer ion interaction model.[20]

Analysis of Experimental Data

Raman spectroscopy can be used for a quantitative analysis of ion speciation if the vibration bands of the individual species can be identified. The assignments of the various SO_4^{2-}, HSO_4^-, and H_3O^+ vibration bands according to Querry et al.[24] and Cox et al.[25] are indicated in Figure 2. We chose the integrated line intensities of the vibration bands $\nu_1(SO_4^{2-})$ at 980 cm^{-1} and $\nu_1(HSO_4^-)$ at 1040 cm^{-1} to obtain the corresponding molal ratio of $m_{SO_4^{2-}}/m_{HSO_4^-}$,[13,15] where m denotes the molality of the

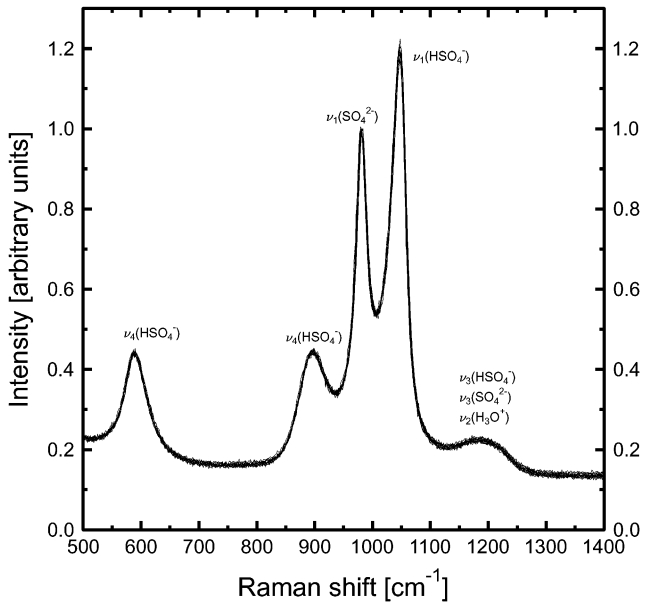

Figure 2. Raman spectra of an aqueous H_2SO_4 droplet 10 μL in volume with a concentration of 4.37 mol kg^{-1} at room temperature. Twelve Raman spectra are shown for which the laser excitation time varies between 1 s and 2 h. Six of the 12 Raman spectra were taken with a laser power of 25 mW. The other six Raman spectra were taken with a laser power of 100 mW. The Raman spectra are normalized to the $\nu_1(SO_4^{2-})$ vibration band.

particular ion. The integrated line intensities, I^ν, were obtained by simultaneously fitting a Lorentzian function to each peak in the 800−1300 cm^{-1} interval. The line intensities are proportional to the concentration of the respective ion i:

$$I^\nu(i) = m(i)\cdot J^\nu(i) \tag{4}$$

where $m(i)$ is the molal concentration and $J^\nu(i)$ is the molal scattering coefficient of ion i. $J^\nu(i)$ depends on the Raman scattering cross section of the ion, $\sigma^\nu(i)$, and on instrumental properties, A_{instr}:

$$J^\nu(i) = \sigma^\nu(i)\cdot A_{\text{instr}} \tag{5}$$

The molal ratio of SO_4^{2-} and HSO_4^- can be derived from the measured integrated line intensities in the following way:

$$\frac{m(SO_4^{2-})}{m(HSO_4^-)} = \frac{J^{1040}(HSO_4^-)}{J^{980}(SO_4^{2-})}\frac{I^{980}(SO_4^{2-})}{I^{1040}(HSO_4)} \tag{6}$$

$$= \frac{\sigma^{1040}(HSO_4^-)A_{\text{instr}}}{\sigma^{980}(SO_4^{2-})A_{\text{instr}}}\frac{I^{980}(SO_4^{2-})}{I^{1040}(HSO_4^-)} \tag{7}$$

$$= \frac{\sigma^{1040}(HSO_4^-)}{\sigma^{980}(SO_4^{2-})}\frac{I^{980}(SO_4^{2-})}{I^{1040}(HSO_4^-)} \tag{8}$$

Therefore, the conversion of an intensity ratio into a molal ratio depends only on the ratio of the Raman scattering cross sections of the particular ions. Equations 6 and 8 show that for one particular experiment the ratio of σ^ν can be substituted by the ratio of the corresponding J^ν, because A_{instr} cancels out. This requires that $\sigma^\nu(i)$ or likewise $J^\nu(i)$ are constant in the investigated concentration and temperature range.

Dawson et al.[13] investigated the temperature and concentration dependence of $J^{980}(SO_4^{2-})$ and $J^{1040}(HSO_4^-)$ using sodium sulfate and ammonium bisulfate solutions. They found both molal scattering coefficients to be constant within 1σ error in the temperature range of 298.15−523.15 K and for concentrations of 0.514−2.25 mol kg^{-1}. Hayes et al.[26] also found that $J^{980}(SO_4^{2-})$ is temperature and concentration independent in the temperature range of 298.15−358.15 K in $(NH_4)_2SO_4/H_2O$ solutions with concentrations of 0.53−3.14 mol kg^{-1}.

Here, we investigate the temperature and concentration dependence of $J^{980}(SO_4^{2-})$ at lower temperatures and higher concentrations than those of the studies mentioned above. The line intensities of the vibration bands $\nu_1(SO_4^{2-})$, $\nu_3(SO_4^{2-})$, and $\nu_4(SO_4^{2-})$ obtained from Raman spectra of $(NH_4)_2SO_4/H_2O$ droplets with concentrations of 0.99−5.35 mol kg^{-1} and at temperatures of 220−296 K were analyzed. Figure 3 displays 10 Raman spectra of a 0.99 mol kg^{-1} $(NH_4)_2SO_4/H_2O$ solution at temperatures between 245 and 285 K and 14 spectra of a 5.35 mol kg^{-1} $(NH_4)_2SO_4/H_2O$ solution at temperatures between 220 and 296 K. The $\nu_3(SO_4^{2-})$ and $\nu_4(SO_4^{2-})$ bands show no change in intensity when compared to the normalized $\nu_1(SO_4^{2-})$ vibration band over the investigated temperature and concentration ranges. We conclude that $J^{980}(SO_4^{2-})$ and, thus, also $\sigma^{980}(SO_4^{2-})$ are constant at temperatures of 220−296 K for concentrations up to 5.35 mol kg^{-1}. Assuming this also to be the case for $J^{1040}(HSO_4^-)$, we can use the measured molal scattering coefficients by Dawson et al.[13] to obtain the ratio of the Raman scattering cross sections: $\sigma^{1040}_{HSO_4^-}/\sigma^{980}_{SO_4^{2-}} = J^{980}(SO_4^{2-})/J^{1040}(HSO_4^-) = 1.035 \pm 0.024$. The small relative difference between the Raman scattering cross sections of 0.035 indicates that the excitations of the SO_4^{2-} and HSO_4^- stretching vibrations are very similar. This gives further support for the above assumption that $J^{1040}(HSO_4^-)$ is independent of temperature and concentration, just as in the case of the investigated $J^{980}(SO_4^{2-})$ band discussed above and in Figure 3.

Figure 4 shows the phase diagram of the H_2SO_4/H_2O system.[27] The temperature and concentration ranges of solutions that were investigated by Raman spectroscopy in this study are indicated by the dashed lines. The experimental data are limited to the temperature range where the droplets remained liquid. As seen in Figure 4, the measurements could be extended well into the supercooled regime. Figure 5 shows Raman spectra of a H_2SO_4/H_2O droplet with a concentration of 2.55 mol kg^{-1} at different temperatures. The spectra are normalized to the $\nu_1(SO_4^{2-})$ vibration band and reveal a strong decrease in the intensity of the $\nu_1(HSO_4^-)$ vibration band at low temperatures. We conclude that the concentration of HSO_4^- decreases with decreasing temperature. The dashed line corresponds to a Raman spectrum of a frozen droplet. The peak at about 3100 cm^{-1} indicates the presence of ice. We also investigated the ratio, R, of the integrated line intensities of the SO_4^{2-} and HSO_4^- vibration bands in the range of 800−1300 cm^{-1} (with a negligible intensity stemming from the $\nu_2(H_3O^+)$ vibration band) and the integrated line intensities of the $\nu_1(H_2O)$ and $\nu_3(H_2O)$ vibration bands in the range of 2500−4000 cm^{-1}, that is

$$R = \frac{\sum_{\nu=800}^{1300} I^\nu(SO_4^{2-}) + I^\nu(HSO_4^-) + I^\nu(H_3O^+)}{\sum_{\nu=2500}^{4000} I^\nu(H_2O)} \tag{9}$$

We found R to be constant for a particular solution concentration over the investigated temperature range within an experimental uncertainty of about 10%, indicating that no concentration changes due to water evaporation or condensation occurred during the cooling of the droplets.

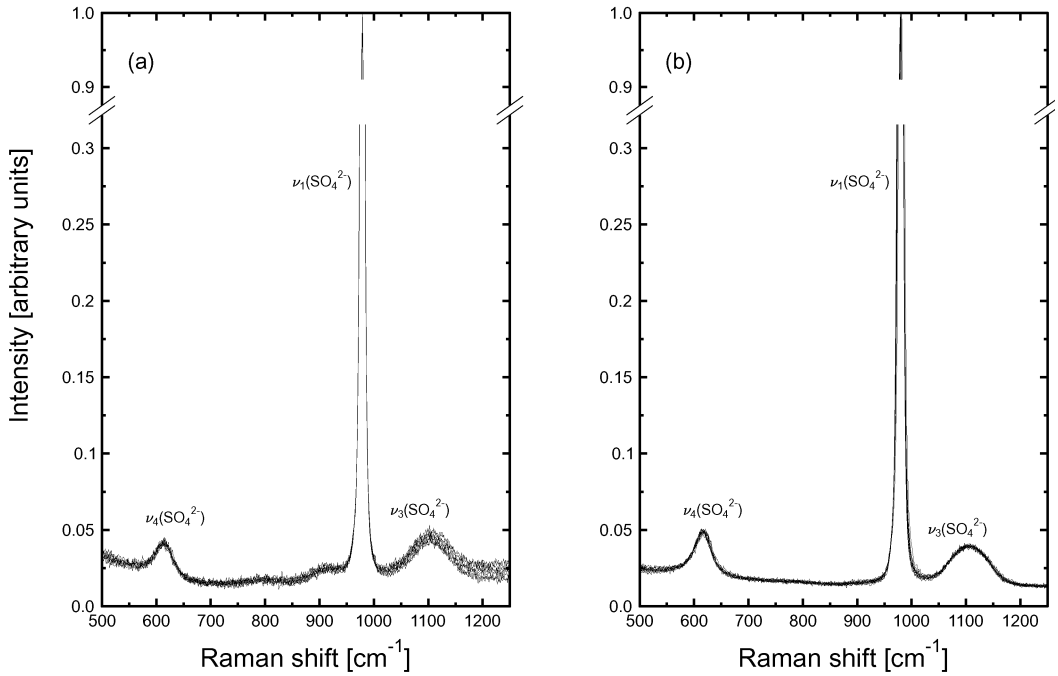

Figure 3. Raman spectra of $(NH_4)_2SO_4/H_2O$ droplets. Panel a shows 10 Raman spectra of a droplet 0.5 μL in volume and with a concentration of 0.99 mol kg^{-1} for temperatures between 245 and 285 K every 5−10 K. Panel b shows 12 Raman spectra of a droplet 1 μL in volume and with a concentration of 5.35 mol kg^{-1} for temperatures between 220 and 296 K every 5−10 K. The Raman spectra are normalized to the $\nu_1(SO_4^{2-})$ vibration band.

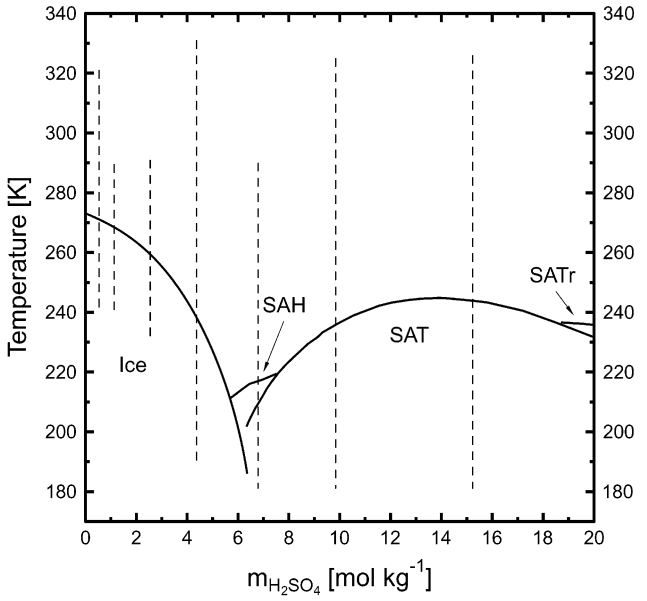

Figure 4. Phase diagram of H_2SO_4/H_2O.[27] Solid lines represent the melting curves of several crystalline solids of H_2SO_4/H_2O: SAH, sulfuric acid hemihexahydrate; SAT, sulfuric acid tetrahydrate; SATr, sulfuric acid trihydrate. The dashed lines indicate the temperatures and concentrations where Raman experiments have been performed.

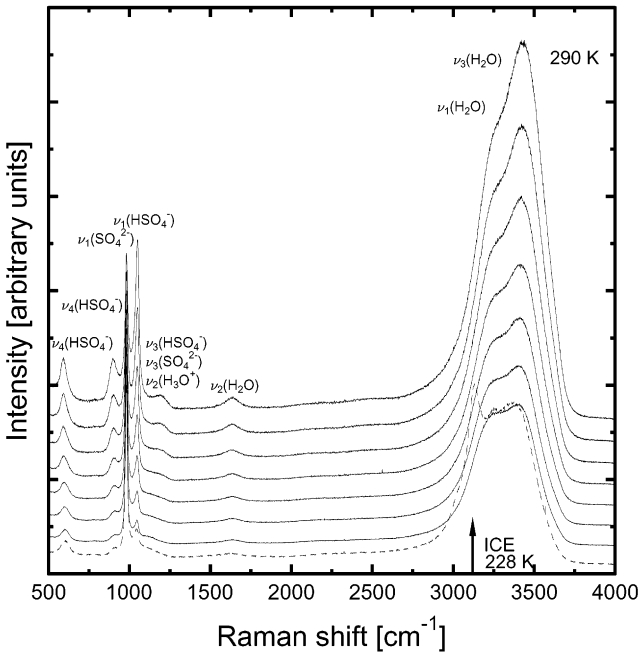

Figure 5. Raman spectra of a H_2SO_4/H_2O droplet 0.5 μL in volume and with a concentration of 2.55 mol kg^{-1}. Spectra are shown from 290 K in 10 K steps until freezing occurs (228 K). The dashed line corresponds to a Raman spectrum of the frozen H_2SO_4/H_2O droplet. Individual spectra are shifted vertically for better visibility. The Raman spectra are normalized to the $\nu_1(SO_4^{2-})$ vibration band.

Figure 6 shows the $m_{SO_4^{2-}}/m_{HSO_4^-}$ ratio obtained from our Raman measurements for 0.54−15.23 mol kg^{-1} H_2SO_4 solutions at temperatures of 180−326 K. The experimental data (open squares) show a continuous increase of the $m_{SO_4^{2-}}/m_{HSO_4^-}$ ratio with decreasing temperature for all investigated concentrations. Tomikawa and Kanno[15] present results which show full dissociation at even lower temperatures for aqueous H_2SO_4 solutions with concentrations of 4.37−15.23 mol kg^{-1} in the glassy state (about 143−158 K). Our Raman data for the 4.37 mol kg^{-1} H_2SO_4 solution are in very good agreement with the data by Tomikawa and Kanno[15] for the same concentration (diamonds in Figure 6). In contrast, the $m_{SO_4^{2-}}/m_{HSO_4^-}$ ratios predicted by the AIM model[19] are much smaller than our measurements and exhibit a maximum for all concentrations at about 180−240 K. In addition, for concentrations greater than 6.79 mol kg^{-1}, the model predictions deviate significantly from the experimental data even at room temperature.

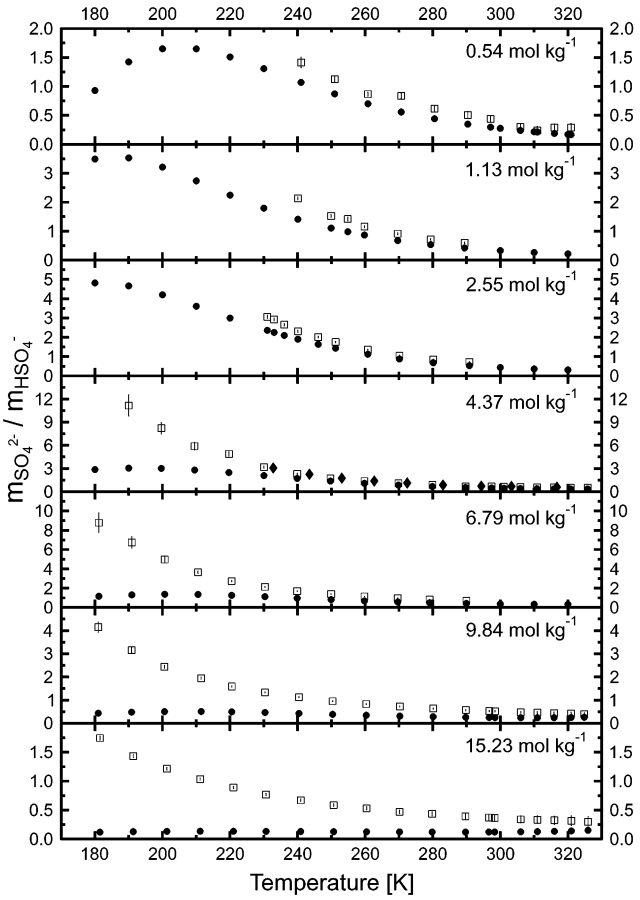

Figure 6. Ratios of $m_{SO_4^{2-}}/m_{HSO_4^-}$ in H_2SO_4/H_2O solutions with concentrations of 0.54−15.23 mol kg^{-1} as a function of temperature. Open squares with error bars indicate the data obtained from our Raman spectra. Circles represent values derived using the AIM model.[19] Diamonds show data of a Raman study by Tomikawa and Kanno.[15] Note the different scales for each concentration.

From the $m_{SO_4^{2-}}/m_{HSO_4^-}$ ratios the degree of dissociation of the HSO_4^- ion, $\alpha_{HSO_4^-}$, can be calculated:

$$\alpha_{HSO_4^-} = \frac{m_{SO_4^{2-}}}{m^{\circ}_{HSO_4^-}} = \frac{m_{SO_4^{2-}}}{m_{HSO_4^-}}\left(1 + \frac{m_{SO_4^{2-}}}{m_{HSO_4^-}}\right)^{-1} \qquad (10)$$

where $m^{\circ}_{HSO_4^-}$ is the total HSO_4^- molality before dissociation.[28] Figure 7 shows $\alpha_{HSO_4^-}$ derived from our experimental data (symbols) as a function of $m_{H_2SO_4}$ for temperatures of 190, 230, and 290 K. The dotted lines correspond to values predicted by the AIM model.[19] The solid lines represent $\alpha_{HSO_4^-}$ values calculated by our Pitzer model (see below). There is a large discrepancy between the experimentally derived data and the AIM values, in particular at low temperatures and high concentrations.

One possible explanation for the observed discrepancy between the AIM model and the experimental data could be an inaccurate parametrization of the thermodynamic dissociation constant of HSO_4^-, $K_{II}(T)$, in the model of Clegg et al.[19] at lower temperatures. The experimental data used to derive the formulation of $K_{II}(T)$ were limited to a temperature range of 298−523 K.[14] Nevertheless, this formulation had been adopted in the AIM model for temperatures down to 180 K. For these reasons we will investigate the temperature dependence of $K_{II}(T)$ in more detail in the following section.

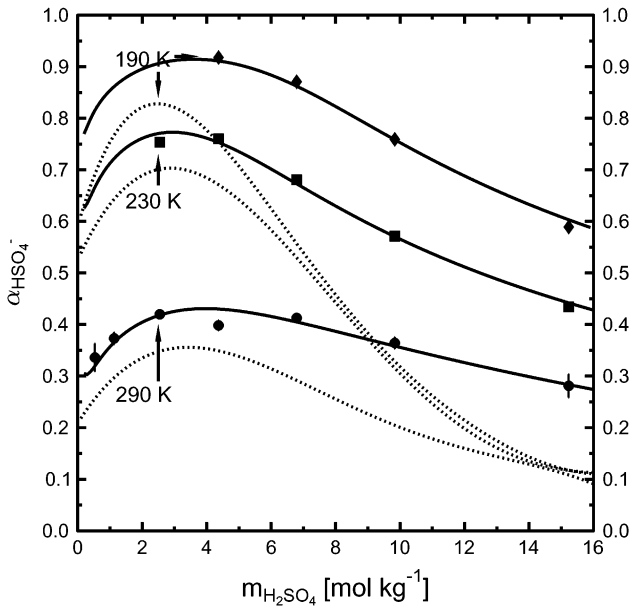

Figure 7. Degree of dissociation of the HSO_4^- ion versus the solution H_2SO_4 molality. Diamonds, squares, and circles with corresponding error bars represent experimentally derived data at 190, 230, and 290 K, respectively. The dotted lines indicate the values predicted by the AIM model.[19] The solid lines show values calculated by the Pitzer ion interaction model using $K_{II}(T)$ derived in this study.

Results of the Pitzer Ion Interaction Model

We have used an extended Pitzer ion interaction model[20] to calculate ion activity coefficients and $K_{II}(T)$ for the H_2SO_4/H_2O system at low temperatures. It is based on the molality concentration scale and is valid up to concentrations of 40 mol kg^{-1}. A detailed description of the working equations is given in the Appendix.

For a consistent calculation of the activity coefficients of the various ions (γ_{H^+}, $\gamma_{SO_4^{2-}}$, $\gamma_{HSO_4^-}$) at low temperatures, the dissociation of HSO_4^- has to be considered. Thus, the temperature dependent second thermodynamic dissociation constant, $K_{II}(T)$, must be known for the investigated temperature range. In Figure 8, ln $K_{II}(T)$ is plotted as a function of inverse temperature. The dotted line shows the formulation of $K_{II}(T)$ given by Clegg et al.,[21] which is also implemented in the AIM model.[19,29] This formulation was originally derived by Dickson et al.[14] for the temperature range of 298−523 K. Some of the high-temperature data of K_{II} of Marshall et al.[30] and Dickson et al.[14] are also plotted as diamonds in Figure 8. The dissociation of HSO_4^- at room and higher temperature is an exothermic reaction. Extrapolation of the formulation of $K_{II}(T)$ of Dickson et al.[14] to low temperatures in the AIM model[19] suggests that the exothermic reaction changes to an endothermic reaction at around 233 K. From $K_{II}(T)$ the corresponding standard Gibbs free energy, $\Delta G^{\dagger}_{II}(T)$, enthalpy, $\Delta H^{\dagger}_{II}(T)$, and entropy, $\Delta S^{\dagger}_{II}(T)$, of the dissociation reaction of HSO_4^- ($HSO_4^- \rightarrow SO_4^{2-} + H^+$) can be derived:

$$\Delta G^{\dagger}_{II}(T) = -RT \ln K_{II}(T) \qquad (11)$$

$$\Delta H^{\dagger}_{II}(T) = -R\frac{\mathrm{d} \ln K_{II}(T)}{\mathrm{d}(1/T)} \qquad (12)$$

$$\Delta S^{\dagger}_{II}(T) = \frac{\Delta H^{\dagger}_{II}(T) - \Delta G^{\dagger}_{II}(T)}{T} \qquad (13)$$

where T is temperature and R is the universal gas constant. The

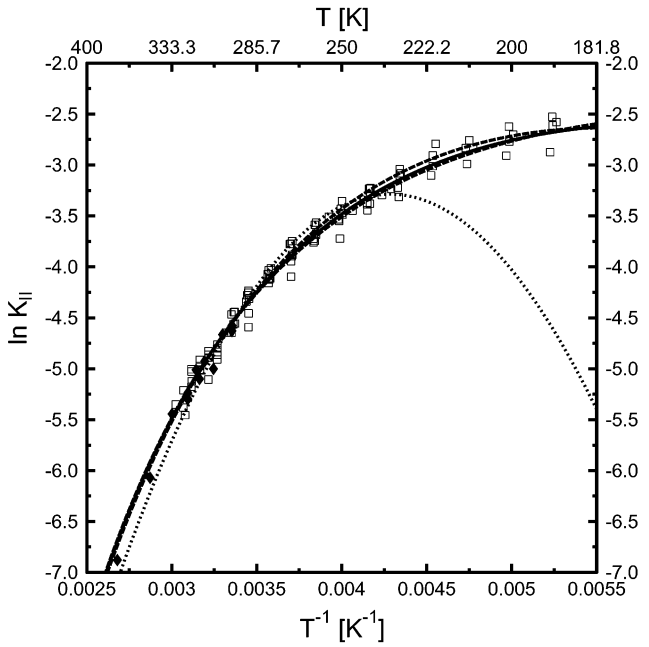

Figure 8. ln K_{II} plotted as a function of inverse temperature. The dotted line corresponds to the formulation given by Clegg et al.[21] The solid line represents K_{II} derived in this study. Dashed lines represent the results of a sensitivity study (see text for details). Open squares show $K_{II}(T)$ values using the measured $\alpha_{HSO_4^-}$ and the activity coefficients derived by our Pitzer model. Diamonds show some of the high-temperature data of K_{II} from Marshall et al.[30] and Dickson et al.[14]

dotted lines in Figure 9 show $\Delta G_{II}^{\dagger}(T)$, $\Delta H_{II}^{\dagger}(T)$, and $\Delta S_{II}^{\dagger}(T)$ for the dissociation reaction of the bisulfate ion using the formulation of $K_{II}(T)$ of Clegg et al.[21] $\Delta G_{II}^{\dagger}$ has a minimum at about 220 K with increasing values at lower temperatures. Also, $\Delta H_{II}^{\dagger}$ and $\Delta S_{II}^{\dagger}$ increase with decreasing temperature over the entire temperature range. $\Delta S_{II}^{\dagger}$ at 298.15 K is about -110 J $K^{-1}mol^{-1}$,[31] which is in agreement with the formulation of $K_{II}(T)$ of Clegg et al.[21] However, the increase in $\Delta S_{II}^{\dagger}$ at very low temperature contradicts the Nernst heat theorem,[32,33] which says that ΔS for any reaction vanishes as temperature approaches 0 K; that is, $\lim_{T\to 0}\Delta S = 0$.

In the following, we use a Pitzer ion interaction model[20] to determine a formulation of $K_{II}(T)$ which is consistent with the experimental data and with thermodynamics. Several data sets were implemented in the Pitzer ion interaction model to obtain the new formulation of $K_{II}(T)$: the data of $\alpha_{HSO_4^-}$ obtained in this study; data of electromotive force experiments;[34] enthalpies and heat capacities of H_2SO_4/H_2O;[35] and dissociation constants in the temperature range of 323−473 K.[14,30] Because each of these data sets consists of a different number of data points, the data were weighted such that each data set had equal weight in the overall fit.

The enthalpy of the dissociation reaction of HSO_4^-, $\Delta H_{II}^{\dagger}(T)$, was fitted within the Pitzer ion interaction model by

$$\Delta H_{II}^{\dagger}(T) = \Delta H_{II}^{\circ} + c_p^{\circ}(T - T_0) + \frac{1}{2}\frac{dc_p}{dT}(T^2 + T_0^2) - \frac{dc_p}{dT}T_0T \quad (14)$$

where T_0 is 298.15 K, ΔH_{II}° is the enthalpy of the dissociation reaction at T_0, c_p° is the heat capacity of the solution at T_0, and dc_p/dT describes its temperature dependence. We performed several model runs to derive a new formulation of $K_{II}(T)$ at low temperatures. To achieve thermodynamic consistence, we were forced to treat the dissociation as an exothermic reaction in the temperature range of 165−473 K in our fitting procedure (i.e. $\Delta H_{II}^{\dagger} \le 0$ for this temperature range). The final results (the parameters for the Pitzer equations and $K_{II}(T)$) are both consistent with all the experimental data and the Nernst heat theorem.[32,33] The formulation for $K_{II}(T)$ derived in this study is shown as the solid line in Figure 8. The dashed lines in Figure 8 indicate the results of a sensitivity study. They represent fits which were constrained to $\Delta H_{II}^{\dagger} \le 0$ down to 120 K and to 180 K, respectively. The two curves (dashed lines) differ only slightly from the best fit (solid line), indicating that the formulation of $K_{II}(T)$ is rather insensitive to the choice of temperature range where $\Delta H_{II}^{\dagger}$ is assumed to be negative. The open squares in Figure 8 were derived using the measured $\alpha_{HSO_4^-}$ and the activity coefficients of the Pitzer model used in the present study. The obtained $K_{II}(T)$ values match the fit, showing that our Pitzer model works in a consistent way. The solid lines in Figure 9 show $\Delta G_{II}^{\dagger}$, $\Delta H_{II}^{\dagger}$, and $\Delta S_{II}^{\dagger}$ calculated using the formulation of $K_{II}(T)$ derived in this study. $\Delta G_{II}^{\dagger}$ decreases with decreasing temperature, and $\Delta H_{II}^{\dagger}$ and $\Delta S_{II}^{\dagger}$ approach zero with decreasing temperature (in the range of available data), in agreement with the Nernst heat theorem.[32,33] It should be noted that, when our new dissociation data are included, the Pitzer model can be tuned to reproduce all

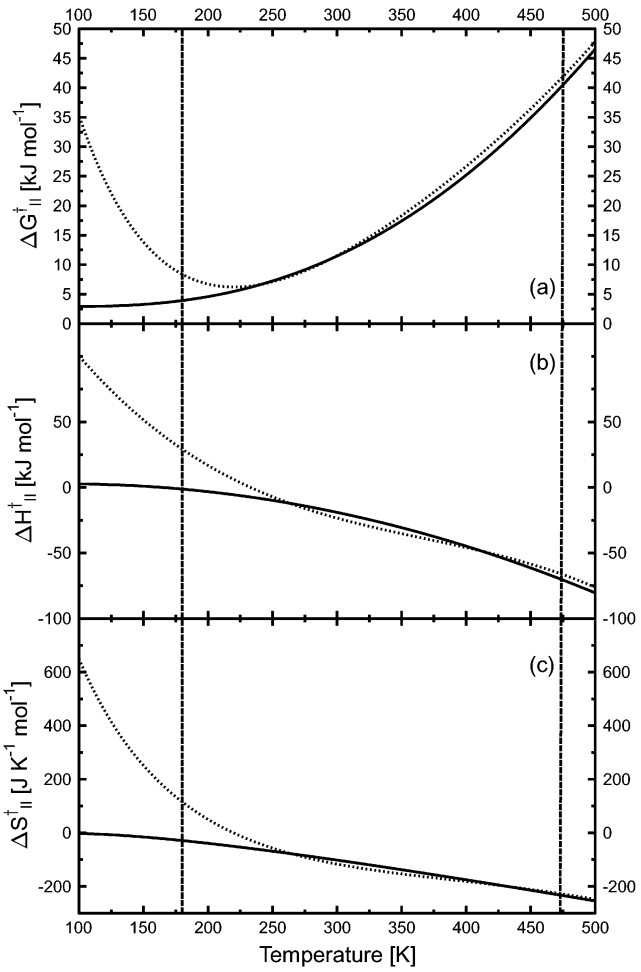

Figure 9. (a) Gibbs free energy for the dissociation reaction of the bisulfate, $\Delta G_{II}^{\dagger}$, as a function of temperature. (b and c) Corresponding reaction enthalpy, $\Delta H_{II}^{\dagger}$, and entropy, $\Delta S_{II}^{\dagger}$, respectively. The dotted lines show results using the formulation of $K_{II}(T)$ by Clegg et al.[21] The solid lines represent results using the formulation of $K_{II}(T)$ derived in this study. The dashed lines indicate the temperature range where experimental data are available.

TABLE 2: Fit Parameters to Derive ln $K_{II}(T)$ Using Eq 16[a]

K°_{II}	$\Delta H^{\circ}_{II}/R$ (K)	c°_{p}/R	$(dc_p/dT)/R$ (K^{-1})
1.0576×10^{-2}	−2231.620 793	−24.7273	−0.119 67

[a] Numerical check: ln $K(273\ K) = -3.954$.

experimental data even with $K_{II}(T)$ fixed to the formulation of Clegg et al.[21] This is achieved by adjusting the ion activity coefficients in the aqueous solutions. However, although the resulting model parametrization is consistent with all experimental data, it contradicts the Nernst heat theorem.[32,33] Furthermore, we expect that also the AIM will reproduce all experimental data, in agreement with the Nernst heat theorem when our new dissociation data and the newly derived $K_{II}(T)$ are implemented. Values for our newly derived $K_{II}(T)$ (solid line in Figure 8) can be calculated from the following equation using the parameters given in Table 2. K_{II} was calculated by integrating eq 12 and using eq 14 for $\Delta H^{\dagger}_{II}$:

$$\ln K_{II}(T) = \ln K^{\circ}_{II}(T_0) - \int_{T_0}^{T} \Delta H^{\dagger}_{II}(T)\, d\frac{1}{T} \quad (15)$$

$$= \ln K^{\circ}_{II} - \left[\left(\Delta H^{\circ}_{II} - c^{\circ}_{p} T_0 + \frac{1}{2}\frac{dc_p}{dT} T_0^{\,2}\right)\left(\frac{1}{T} - \frac{1}{T_0}\right) - \left(c^{\circ}_{p} - \frac{dc_p}{dT} T_0\right) \ln \frac{T}{T_0} - \frac{1}{2}\frac{dc_p}{dT}(T - T_0)\right] \quad (16)$$

The above formulation can be used in the temperature range of 180−473 K.

With the newly derived formulation for $K_{II}(T)$ our Pitzer ion interaction model can be used to predict the degree of dissociation, $\alpha^{mod}_{HSO_4^-}$. Comparisons between the modeled $\alpha^{mod}_{HSO_4^-}$ and the experimentally obtained data are given in Table 3 and Figure 7. Also shown in Table 3 are values for the activity coefficient

TABLE 3: Experimental Data and Modeling Results for the Investigated Aqueous H_2SO_4 Solutions[a]

T (K)	H_2SO_4 (mol kg^{-1})	$\alpha_{HSO_4^-}$	$\alpha^{mod}_{HSO_4^-}$	ln Q	ln γ	T (K)	H_2SO_4 (mol kg^{-1})	$\alpha_{HSO_4^-}$	$\alpha^{mod}_{HSO_4^-}$	ln Q	ln γ
321.0	0.54	0.22	0.20	−1.667	−3.507	269.6	6.79	0.49	0.48	2.280	−6.124
316.0	0.54	0.22	0.22	−1.657	−3.379	259.8	6.79	0.53	0.52	2.473	−6.093
311.0	0.54	0.19	0.23	−1.864	−3.033	249.9	6.79	0.58	0.57	2.703	−6.110
306.0	0.54	0.23	0.25	−1.620	−3.140	239.9	6.79	0.63	0.62	2.926	−6.131
297.1	0.54	0.30	0.29	−1.182	−3.344	230.3	6.79	0.68	0.67	3.193	−6.222
290.4	0.54	0.34	0.32	−1.014	−3.337	220.5	6.79	0.73	0.72	3.471	−6.334
280.5	0.54	0.38	0.37	−0.787	−3.318	210.5	6.79	0.78	0.77	3.789	−6.503
270.7	0.54	0.46	0.42	−0.424	−3.444	200.7	6.79	0.83	0.82	4.125	−6.714
260.8	0.54	0.46	0.48	−0.384	−3.258	190.9	6.79	0.87	0.86	4.451	−6.940
251.0	0.54	0.53	0.54	−0.079	−3.350	181.2	6.79	0.90	0.89	4.729	−7.145
241.0	0.54	0.59	0.60	0.185	−3.413	324.9	9.84	0.28	0.29	1.612	−6.897
289.4	1.13	0.37	0.37	−0.077	−4.251	320.9	9.84	0.30	0.30	1.682	−6.856
279.4	1.13	0.42	0.42	0.135	−4.212	315.9	9.84	0.31	0.31	1.730	−6.764
269.6	1.13	0.48	0.48	0.418	−4.261	311.0	9.84	0.32	0.31	1.790	−6.687
259.8	1.13	0.54	0.54	0.696	−4.315	306.1	9.84	0.32	0.32	1.814	−6.578
254.9	1.13	0.59	0.57	0.937	−4.448	298.4	9.84	0.34	0.34	1.931	−6.490
249.9	1.13	0.60	0.60	1.019	−4.427	296.7	9.84	0.35	0.34	1.945	−6.460
240.1	1.13	0.68	0.66	1.401	−4.611	289.8	9.84	0.36	0.36	2.040	−6.376
290.8	2.55	0.42	0.41	0.962	−5.325	280.1	9.84	0.39	0.38	2.161	−6.256
280.1	2.55	0.46	0.47	1.144	−5.239	270.3	9.84	0.42	0.41	2.316	−6.174
270.1	2.55	0.51	0.52	1.398	−5.253	260.3	9.84	0.45	0.45	2.471	−6.102
260.8	2.55	0.57	0.58	1.690	−5.332	250.4	9.84	0.49	0.48	2.634	−6.051
251.2	2.55	0.64	0.64	1.989	−5.423	240.4	9.84	0.53	0.52	2.829	−6.045
246.1	2.55	0.67	0.68	2.145	−5.474	230.4	9.84	0.57	0.57	3.025	−6.054
240.1	2.55	0.70	0.71	2.304	−5.513	220.5	9.84	0.61	0.61	3.226	−6.089
236.1	2.55	0.73	0.74	2.457	−5.589	211.5	9.84	0.66	0.66	3.459	−6.186
233.0	2.55	0.75	0.75	2.565	−5.643	200.6	9.84	0.71	0.71	3.712	−6.300
231.0	2.55	0.75	0.77	2.615	−5.656	190.8	9.84	0.76	0.75	3.999	−6.488
325.9	4.37	0.34	0.33	1.093	−6.407	181.0	9.84	0.81	0.80	4.301	−6.716
320.8	4.37	0.34	0.34	1.112	−6.283	326.0	15.23	0.23	0.23	1.718	−7.034
315.9	4.37	0.35	0.35	1.156	−6.189	321.0	15.23	0.24	0.24	1.784	−6.961
310.9	4.37	0.36	0.36	1.208	−6.103	316.0	15.23	0.25	0.24	1.817	−6.854
306.0	4.37	0.37	0.38	1.276	−6.037	311.0	15.23	0.25	0.25	1.848	−6.746
301.0	4.37	0.39	0.39	1.344	−5.973	306.1	15.23	0.25	0.26	1.868	−6.631
297.4	4.37	0.40	0.40	1.397	−5.931	298.3	15.23	0.27	0.27	1.948	−6.505
289.7	4.37	0.40	0.43	1.398	−5.733	296.6	15.23	0.27	0.27	1.971	−6.483
279.9	4.37	0.47	0.47	1.748	−5.837	289.7	15.23	0.28	0.28	2.032	−6.366
269.8	4.37	0.52	0.52	1.982	−5.830	279.8	15.23	0.30	0.30	2.156	−6.243
259.8	4.37	0.58	0.58	2.250	−5.869	270.2	15.23	0.32	0.32	2.244	−6.100
249.7	4.37	0.64	0.64	2.522	−5.926	260.4	15.23	0.35	0.35	2.391	−6.024
239.9	4.37	0.70	0.70	2.844	−6.050	250.7	15.23	0.37	0.38	2.502	−5.925
230.0	4.37	0.76	0.75	3.195	−6.218	240.9	15.23	0.40	0.41	2.662	−5.888
219.7	4.37	0.83	0.81	3.665	−6.515	230.7	15.23	0.43	0.44	2.819	−5.854
209.5	4.37	0.85	0.85	3.867	−6.568	221.0	15.23	0.47	0.47	2.994	−5.865
199.7	4.37	0.89	0.89	4.219	−6.797	211.2	15.23	0.51	0.51	3.170	−5.893
190.0	4.37	0.92	0.91	4.540	−7.021	201.3	15.23	0.55	0.55	3.355	−5.951
289.9	6.79	0.41	0.41	1.909	−6.249	191.3	15.23	0.59	0.60	3.546	−6.039
279.1	6.79	0.45	0.44	2.082	−6.151	181.5	15.23	0.64	0.64	3.771	−6.190

[a] The first two columns indicate the temperature and concentration of the H_2SO_4 solutions. $\alpha_{HSO_4^-}$ is the experimentally obtained degree of dissociation (see eq 10); $\alpha^{mod}_{HSO_4^-}$ is the degree of dissociation calculated from our Pitzer model using the new $K_{II}(T)$ formulation; Q is the molal equilibrium quotient (see eq 3); γ is the activity coefficient product (see eq 3).

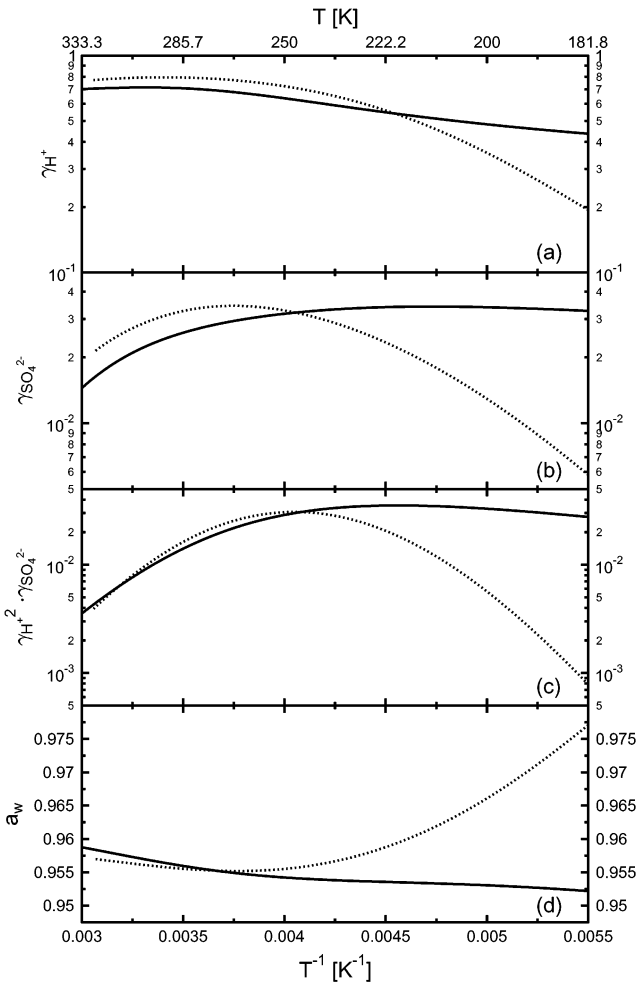

Figure 10. Activity coefficients γ_{H^+}, $\gamma_{SO_4^{2-}}$, $\gamma_{H^+}^2 \cdot \gamma_{SO_4^{2-}}$, and a_w of a 1.13 mol kg^{-1} H_2SO_4/H_2O solution plotted as a function of inverse temperature. The solid lines are calculated by the Pitzer model using $K_{II}(T)$ derived in this study. The dotted lines are predictions from the AIM model by Clegg et al.[19]

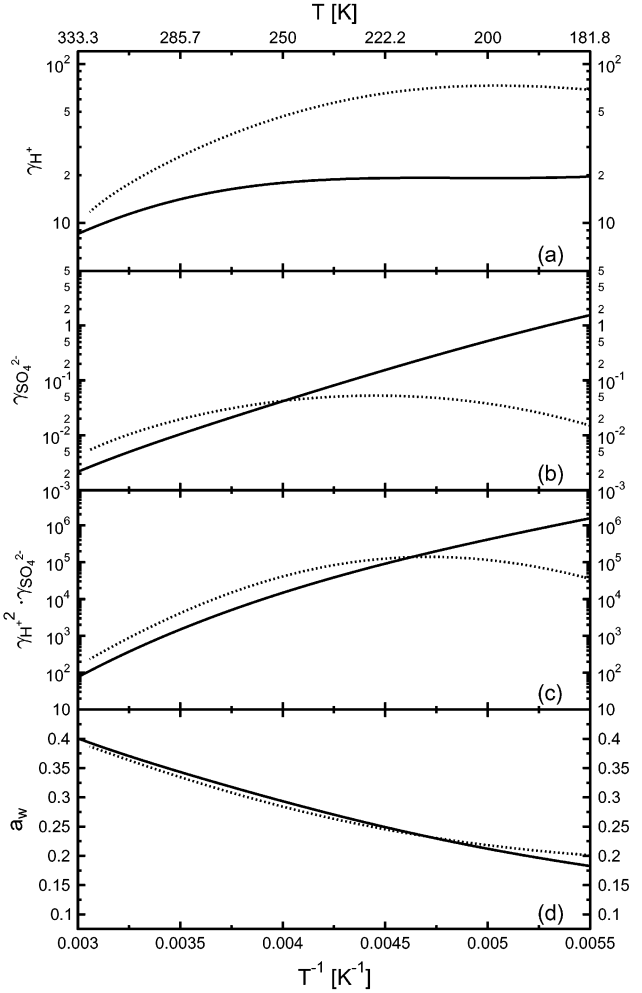

Figure 11. Activity coefficients γ_{H^+}, $\gamma_{SO_4^{2-}}$, $\gamma_{H^+}^2 \cdot \gamma_{SO_4^{2-}}$, and a_w of a 9.84 mol kg^{-1} H_2SO_4/H_2O solution plotted as a function of inverse temperature. The solid lines are calculated by the Pitzer model using $K_{II}(T)$ derived in this study. The dotted lines are predictions from the AIM model by Clegg et al.[19]

product, $\gamma(T)$, which were calculated from eq 3 using the $K_{II}(T)$ values from eq 16 together with $Q(T)$ values obtained directly from the experimental data.

Figures 10 and 11 show calculated ion activity coefficients, γ_{H^+}, $\gamma_{SO_4^{2-}}$, and $\gamma_{H^+}^2 \cdot \gamma_{SO_4^{2-}}$, and water activities, a_w, for a 1.13 mol kg^{-1} and a 9.84 mol kg^{-1} H_2SO_4/H_2O solution, respectively. The solid lines correspond to values calculated with our Pitzer model using the new $K_{II}(T)$ formulation; the dotted lines are calculated using the AIM model.[19] Significant differences between the two models exist for all parameters, in particular at low temperatures. Note that the difference in a_w for the 9.84 mol kg^{-1} solution is about 10% at 180 K. This may be due to the larger HSO_4^- dissociation and, thus, larger ionic strength in our model at low temperatures. Also note that the activity coefficients between the two models also differ strongly, for example in the case of $\gamma_{SO_4^{2-}}$ in Figure 11b by up to 2 orders of magnitude.

Atmospheric Implications

Relative humidity and temperature can vary over a large range in the atmosphere; for example, temperatures can be as low as 180 K in the polar stratosphere and tropical tropopause. Stratospheric aerosols can consist of highly concentrated H_2SO_4/H_2O droplets[6,7] at dry conditions. Under these conditions the experimental data obtained in this work show a significantly higher dissociation for the reaction $HSO_4^- \rightleftharpoons SO_4^{2-} + H^+$ than was assumed in previous model calculations. This also has implications for other thermodynamic properties of aqueous H_2SO_4 solutions. The water vapor pressure, p_{H_2O}, of a H_2SO_4/H_2O solution depends on the water activity of the solution, a_w:

$$p_{H_2O}(T) = a_w(T) p^\circ_{H_2O}(T) \qquad (17)$$

where $p^\circ_{H_2O}$ is the water vapor pressure over pure water at the same temperature. Because we calculate lower water activities at low temperatures than the AIM does, our results imply slightly lower water vapor pressures of sulfuric acid aerosols under stratospheric conditions.

In addition, the new binary interaction parameters for H_2SO_4/H_2O obtained by our Pitzer model can serve as input parameters for the derivation of ternary interaction parameters in aqueous solutions such as the $NH_3/H_2SO_4/H_2O$ and $HCl/H_2SO_4/H_2O$ systems, which are common in aerosols of the troposphere and stratosphere. Furthermore, the solubility of trace gases in H_2SO_4/H_2O solutions such as HCl and NH_3 is affected.[9,10] The larger dissociation constant leads to higher H^+ concentrations in H_2SO_4/H_2O solutions and, therefore, to lower HCl solubilities/Henry's law constants when compared to AIM

results.[23] Over the concentration range of 4.3−15.23 mol kg^{-1} and at temperatures between 180 and 300 K, the maximum difference between our model and the AIM[23] is about a factor of 3. We note that Carslaw et al.[23] show in their Figure 13 that data from vapor pressure measurements[36,37] fall below their model predictions, while data from uptake experiments[36,38,39] are closer to predictions. Later Hanson et al.[40] reexamined their earlier data, which are still below but closer to the predictions than before. Unfortunately, the scatter between the different data sets (and experimental methods) is large and, thus, does not allow us to conclude which of the model predictions is closer to real solubilities at this stage.

Conclusions

The dissociation of the bisulfate ion ($HSO_4^- \rightleftharpoons SO_4^{2-} + H^+$) has been studied in a temperature range of 180−326 K in H_2SO_4 solutions with concentrations of 0.54−15.23 mol kg^{-1} using Raman spectroscopy. The experimental results show a continuous increase in the degree of dissociation of HSO_4^- with decreasing temperatures within the investigated concentration and temperature range. Our results disagree with predictions from the thermodynamic model AIM,[19] which underestimates the degree of dissociation of HSO_4^- for high H_2SO_4 concentrations and low temperatures by up to a factor of 5. This is most likely due to the implementation of a thermodynamic dissociation constant in the AIM, that is at odds with the Nernst heat theorem. Therefore, we have employed a Pitzer ion interaction model to obtain a new thermodynamically consistent formulation of the thermodynamic dissociation constant, $K_{II}(T)$, that is in agreement with experimental data. The new formulation of $K_{II}(T)$ is valid from 180 to 473 K. In the model, consistency with thermodynamics can be achieved only by assuming that the dissociation reaction is exothermic over the entire temperature range. Results from our model indicate that ion activity coefficients can differ by up to 2 orders of magnitude, water activities and vapor pressures by up to 10%, and HCl solubilities by up to a factor 3 when compared to results from the AIM.[19,23]

We recommend that future thermodynamic investigations of multicomponent aqueous solutions containing H_2SO_4 use the new formulation of $K_{II}(T)$ for a correct description of the dissociation reaction of the bisulfate ion.

Appendix

Derivation of the Thermodynamic Dissociation Constant of HSO_4^-. The chemical potentials μ_i ($i = H^+, SO_4^{2-}, HSO_4^-$) of the species involved in the dissociation reaction $HSO_4^- \rightleftharpoons SO_4^{2-} + H^+$ can be written as

$$\mu_i(T) = \mu_i^\dagger(T) + RT \ln a_i(T) \tag{18}$$

where $\mu_i^\dagger$ is the standard chemical potential of the species i, that is, the chemical potential in a hypothetical 1 mol kg^{-1} aqueous solution with ideal properties. The activity, a_i, of each species is the product of its activity coefficient, γ_i, and its molality m_i, such that $a_i(T) = \gamma_i(T)(m_i(T)/m^\dagger)$. $m^\dagger$ is by definition 1 mol kg^{-1}.

In chemical equilibrium, the Gibbs free energy for the dissociation reaction is

$$\Delta G_{II}(T) = \mu_{SO_4^{2-}}(T) + \mu_{H^+}(T) - \mu_{HSO_4^-}(T) = 0 \tag{19}$$

Replacing μ_i from eqs 18 and 11 into eq 19 yields the temperature dependent thermodynamic dissociation constant of HSO_4^-, $K_{II}(T)$:

$$K_{II}(T) = \left(\frac{m_{SO_4^{2-}}(T) m_{H^+}(T)}{m_{HSO_4^-}(T) m^\dagger}\right)\left(\frac{\gamma_{SO_4^{2-}}(T)\gamma_{H^+}(T)}{\gamma_{HSO_4^-}(T)}\right) \tag{20}$$

Equation 20 shows that in order to derive $K_{II}(T)$ not only dissociation data are required, but also knowledge of the activity coefficients of the involved ions.

Extended Pitzer Ion Interaction Model. The Gibbs free energy of an aqueous electrolyte solution can be written as

$$\frac{G}{w_w RT} = \frac{1}{RT}[\Omega(\mu_w - \mu_w^\dagger) + \sum_i m_i(\mu_i - \mu_i^\dagger)] \tag{21}$$

$$= \Omega \ln a_w + \sum_i m_i \ln a_i \tag{22}$$

where R is the universal gas constant, T is the temperature, w_w is the mass of the solvent (1 kg of water), Ω is the number of moles in 1 kg of water (55.51 mol), and m_i, μ_i, $\mu_i^\dagger$, and a_i are defined as above.

For an ideal solution, the activity coefficient $\gamma_i = 1$ and, thus, the Gibbs free energy of an ideal solution becomes

$$\frac{G^{ideal}}{w_w RT} = \Omega \ln a_w^{ideal} + \sum_i m_i \ln\left(\frac{m_i}{m^\dagger}\right) \tag{23}$$

Since the excess Gibbs free energy is the difference between the Gibbs free energies of a real and an ideal solution, one finds using eqs 22 and 23

$$\frac{G^{ex}}{w_w RT} = \frac{G}{w_w RT} - \frac{G^{ideal}}{w_w RT} \tag{24}$$

$$= \Omega(\ln a_w - \ln a_w^{ideal}) + \sum_i m_i \ln \gamma_i \tag{25}$$

Instead of water activity, the osmotic coefficient, Φ, is often used in thermodynamic treatments and is defined as

$$\Phi = -\frac{\Omega}{\sum_i m_i} \ln a_w \tag{26}$$

To derive the water activity in the ideal solution, a_w^{ideal}, the Gibbs−Duhem relation is applied to eq 23:

$$\Omega d \ln a_w^{ideal} + \sum_i m_i d \ln\left(\frac{m_i}{m^\dagger}\right) = 0 \tag{27}$$

and integration yields

$$\ln a_w^{ideal} = -\frac{1}{\Omega}\sum_i m_i \tag{28}$$

Thus, eq 25 can be written as

$$\frac{G^{ex}}{w_w RT} = \sum_i m_i(1 - \Phi + \ln \gamma_i) \tag{29}$$

The water activity, a_w, and the activity coefficients, γ_i ($i = H^+$,

TABLE 4: Temperature Dependent Parameters (p) and Temperature Independent Parameters (α_{ca}, ω_{ca}, b) of the Ion Interaction Model[a]

p	χ	$\Delta H^{\circ}_{II}/R$ (K)	c°_p/R	$(dc_p/dT)/R$ (K^{-1})
$\beta^{(0)}_{H^+,HSO_4^-}$	−0.12672773	122.83352564	0.79298257	4.49770×10^{-3}
$\beta^{(1)}_{H^+,HSO_4^-}$	1.43843400	140.47112887	−15.44397569	−0.49178043
$c^{(0)}_{H^+,HSO_4^-}$	1.08965×10^{-3}	−1.36879879	-9.58811×10^{-3}	-2.78×10^{-6}
$c^{(1)}_{H^+,HSO_4^-}$	0.31617615	4.38280351	−0.50421020	2.74165×10^{-3}
$\beta^{(0)}_{H^+,SO_4^{2-}}$	0.12485773	9.86603452	−0.59448781	-6.1367×10^{-4}
$\beta^{(1)}_{H^+,SO_4^{2-}}$	−0.46260131	358.49482175	17.75619395	5.849624×10^{-2}
$c^{(0)}_{H^+,SO_4^{2-}}$	5.10014×10^{-3}	−3.21170454	-1.264739×10^{-2}	-4.46×10^{-6}
$c^{(1)}_{H^+,SO_4^{2-}}$	−0.27604369	83.11418947	4.55227587	6.408755×10^{-2}
b_{H^+,HSO_4^-}:	1.2		$b_{H^+,SO_4^{2-}}$:	1.2
ω_{H^+,HSO_4^-}:	0.91291829		$\omega_{H^+,SO_4^{2-}}$:	1.91623572
α_{H^+,HSO_4^-}:	2.0		$\alpha_{H^+,SO_4^{2-}}$:	2.0

[a] Units are as follows: $\beta^{(0)}_{ca}$ and $\beta^{(1)}_{ca}$ in kg mol^{-1}; $c^{(0)}_{ca}$ and $c^{(1)}_{ca}$ in kg^2 mol^{-2}; α_{ca}, ω_{ca}, and b_{ca} in $kg^{1/2}$ $mol^{-1/2}$. The temperature dependent parameters are calculated in the following way: $p = \ln \chi + (\Delta H^{\circ}_{II} - c^{\circ}_p T_0 + {}^1/_2(dc_p/dT)T_0^2)((1/T) - (1/T_0)) - (c^{\circ}_p - (dc_p/dT)T_0) \ln(T/T_0) - {}^1/_2(dc_p/dT)(T - T_0)$.

SO_4^{2-}, HSO_4^-), can be derived from the following derivatives of the excess Gibbs free energy:

$$\ln a_w = \frac{1}{RT}\left(\frac{\partial G^{ex}}{\partial(\Omega w_w)}\right) + \ln a_w^{ideal} \tag{30}$$

$$\ln \gamma_i = \frac{1}{RT}\left(\frac{\partial G^{ex}/w_w}{\partial m_i}\right) \tag{31}$$

Using eqs 26, 28, and 30, the expression for the osmotic coefficient can be written as

$$\Phi - 1 = -\frac{1}{\sum_i m_i}\frac{1}{RT}\left(\frac{\partial G^{ex}}{\partial w_w}\right) \tag{32}$$

The statistical mechanics of electrolytic solutions suggest that G^{ex} can be expressed in terms of a virial expansion in concentration.[20] In our model the three-body interaction (H^+, SO_4^{2-}, HSO_4^-) and the interaction between HSO_4^- and SO_4^{2-} are neglected and, therefore, G^{ex} can be written as

$$\frac{G^{ex}}{w_w RT} \simeq f(I) + \sum_{ca} m_c m_a (2B_{ca}(I) + ZC_{ca}(I)) \tag{33}$$

where m_i is the molality of the ith ion (i = a or c, i.e., anion or cation, respectively). Z is given by $Z = \sum_i |m_i z_i|$, where z_i is the charge of the ith ion. $f(I)$ is the Debye−Hückel term, representing the long-range electrostatic interaction, and $B_{ca}(I)$ and $C_{ca}(I)$ describe the short-range interactions in binary solutions. $B_{ca}(I)$ is the two-body interaction term (one cation interacts with one anion), and $C_{ca}(I)$ is the three-body interaction term (two identical ions interact with one other ion: cca, aac). All given parameters depend on temperature and on the molal ionic strength, I, which is given by $I = {}^1/_2 \sum_i m_i z_i^2$.

According to eq 31 the activity coefficient of a cation or an anion can be derived by taking the derivatives from eq 33:

$$\ln \gamma_c = z_c^2 F + \sum_a m_a (2B_{ca} + ZC_{ca}) \tag{34}$$

$$\ln \gamma_a = z_a^2 F + \sum_c m_c (2B_{ca} + ZC_{ca}) \tag{35}$$

where the summations run over cations (c) and anions (a). The quantity F includes derivatives of the long-range electrostatic interaction term, f, and of B and C with respect to the ionic strength I:

$$F = \frac{1}{2}f' + \sum_{ca} m_c m_a \left(B'_{ca} + \frac{Z}{2}C'_{ca}\right) \tag{36}$$

According to eq 32 the osmotic coefficient is calculated from the derivative of eq 33 with respect to w_w:

$$\Phi - 1 = -\frac{2}{\sum_i m_i}[If^{\Phi}(I) + \sum_{ca} m_c m_a [B^{\Phi}_{ca}(I) + ZC^{\Phi}_{ca}(I)]] \tag{37}$$

where

$$f^{\Phi}(I) = \frac{1}{2I}(If'(I) - f(I)) \tag{38}$$

$$B^{\Phi}_{ca}(I) = B_{ca}(I) + IB'_{ca}(I) \tag{39}$$

$$C^{\Phi}_{ca}(I) = C_{ca}(I) + \frac{I}{2}C'_{ca}(I) \tag{40}$$

The differential equations 38-40 are solved numerically using the following analytical functions fitted to available data sets:

$$f^{\Phi}(I) = -\frac{A^{\phi} I^{1/2}}{1 + bI^{1/2}} \tag{41}$$

$$B^{\Phi}_{ca}(I) = \beta^{(0)}_{ca} + \beta^{(1)}_{ca} e^{-\alpha\sqrt{I}} \tag{42}$$

$$C^{\Phi}_{ca}(I) = c^{(0)}_{ca} + c^{(1)}_{ca} e^{-\omega\sqrt{I}} \tag{43}$$

where A^{ϕ} is the temperature dependent Debye−Hückel parameter given by Pitzer,[20] and $\beta^{(0)}_{ca}$, $\beta^{(1)}_{ca}$, $c^{(0)}_{ca}$, and $c^{(1)}_{ca}$ are temperature dependent fit parameters, and b, α, and ω are temperature independent fit parameters. Note that the parameters $c^{(0)}_{ca}$ and $c^{(1)}_{ca}$ represent the average of the two different three-body interactions caa and cca, which cannot be separated numerically. The analytical functions f^{Φ} and B^{Φ}_{ca} in eqs 41 and 42 are chosen according to Pitzer[20] to yield the best fit to the data of a large number of aqueous solutions. We chose C^{Φ}_{ca} also to depend on the ionic strength. The parameters of our Pitzer ion interaction model are given in Table 4.

The solutions of the differential equations 38, 39, and 40 give $f(I)$, $B_{ca}(I)$, $C_{ca}(I)$, and their corresponding derivatives. These

functions are required to calculate a_w using eq 37 or to derive the activity coefficients employing eqs 34 and 35.

Acknowledgment. Helpful discussion with H. Kanno and Th. Peter and technical support of U. G. Weers are gratefully acknowledged. This work was funded through an internal ETH grant.

References and Notes

(1) Donovan, J. R.; Salamone, J. M. Sulfuric Acid and Sulfur Trioxide. In *Sulfonation and Sulfation to Thorium and Thorium Compounds*, 3rd ed.; Grayson, M., Ed.; Wiley & Sons: New York, 1983; Vol. 22.

(2) Rard, J. A.; Habenschuss, A.; Spedding, F. H. *J. Chem. Eng. Data* **1976**, *21*, 374−379.

(3) Staples, B. R. *J. Phys. Chem. Ref. Data* **1981**, *10*, 779−798.

(4) Bolsaitis, P.; Elliott, J. F. *J. Chem. Eng. Data* **1990**, *35*, 69−85.

(5) Zeleznik, F. J. *J. Phys. Chem. Data* **1991**, *20*, 1157−1200.

(6) Junge, C. E.; Manson, J. E. *J. Geophys. Res.* **1961**, *66*, 2163-2182.

(7) Hamill, P.; Toon, O. B. *Phys. Today* **1991**, *44*, 34−42.

(8) Murphy, D. M.; Thomson, D. S.; Mahoney, T. M. J. *Science* **1998**, *282*, 1664−1669.

(9) Luo, B. P.; Clegg, S. L.; Peter, T.; Müller, R.; Crutzen, P. J. *Geophys. Res. Lett.* **1994**, *21*, 49−52.

(10) Swartz, E.; Shi, Q.; Davidovits, P.; Jayne, J. T.; Worsnop, D. R.; Kolb, C. E. *J. Phys. Chem. A* **1999**, *103*, 8824−8833.

(11) Young, T. F.; Maranville, L. F.; Smith, H. M. Raman Spectral Investigations of Ionic Equilibria in Solutions of Strong Electrolytes. In *The Structure of Electrolyte Solutions*; Hamer, W. J., Ed.; Wiley: New York, 1959.

(12) Chen, H.; Irish, D. E. *J. Phys. Chem.* **1971**, *75*, 2672−2681.

(13) Dawson, B. S. W.; Irish, D. E.; Toogood, G. E. *J. Phys. Chem.* **1986**, *90*, 334−341.

(14) Dickson, A. G.; Weolowski, D. J.; Palmer, D. A.; Mesmer, R. E. *J. Phys. Chem.* **1990**, *94*, 7978−7985.

(15) Tomikawa, K.; Kanno, H. *J. Phys. Chem.* **1998**, *102*, 6082−6088.

(16) Zhang, R.; Woolridge, P. J.; Abatt, J. D. P.; Molina, M. J. *J. Phys. Chem.* **1993**, *97*, 7351−7358.

(17) Massucci, M.; Clegg, S. L.; Brimblecombe, P. *J. Chem. Eng. Data* **1996**, *41*, 765−778.

(18) Das, A.; Dev, S.; Shangpliang, H.; Nonglait, K.; Ismail, K. *J. Phys. Chem. B* **1997**, *101*, 4166−4170.

(19) Clegg, S. L.; Brimblecombe, P.; Wexler, A. S. *J. Phys. Chem. A* **1998**, *102*, 2137−2154; http://www.hpc1.uea.ac.uk/e770/aim.html.

(20) Pitzer, K. S. *Activity Coefficients in Electrolyte Solutions*, 2nd ed.; CRC Press: Boca Raton, FL, 1991.

(21) Clegg, S. L.; Rard, J. A.; Pitzer, K. S. *J. Chem. Soc., Faraday Trans.* **1994**, *90*, 1875−1894.

(22) Knopf, D. A.; Koop, T.; Luo, B. P.; Weers, U. G.; Peter, T. *Atmos. Chem. Phys.* **2002**, *2*, 207−214.

(23) Carslaw, K. S.; Clegg, S. L.; Brimblecombe, P. *J. Phys. Chem.* **1995**, *99*, 11557−11574; http://www.hpc1.uea.ac.uk/e770/aim.html.

(24) Querry, M. R.; Waring, R. C.; Holland, W. E.; Earls, L. M.; Herrman, M. D.; Nijm, W. P.; Hale, G. M. *J. Opt. Soc. Am.* **1974**, *64*, 39−46.

(25) Cox, R. A.; Haldna, U. L.; Idler, K. L.; Yates, K. *Can. J. Chem.* **1981**, *59*, 2591−2598.

(26) Hayes, A. C.; Kruus, P.; Adams, W. A. *J. Solution Chem.* **1984**, *13*, 61−75.

(27) Gable, C. M.; Betz, H. F.; Maron, S. H. *J. Am. Chem. Soc.* **1950**, *72*, 1445−1448.

(28) $m^{\circ}_{HSO_4^-}$ is assumed to be equal to the total H_2SO_4 molality, although this assumption is not required to derive $\alpha_{HSO_4^-}$.

(29) In ref 19 $K_{II}(T)$ was transformed from molality to mole fraction scale.

(30) Marshall, W. L.; Jones, E. V. *J. Phys. Chem.* **1966**, *70*, 4028−4040.

(31) Lide, D. R., Ed. *CRC Handbook of Chemistry and Physics*, 79th ed.; CRC Press: New York, 1998.

(32) Nernst, W. *Nachr. Ges. Wiss. Göttingen, Math.-Phys. Kl.* **1906**, 1−40.

(33) Berry, R. S.; Stuart, A. R.; Ross, J. *Physical Chemistry (Topics in Physical Chemistry)*, 2nd ed.; John Wiley & Sons: New York, 2000.

(34) Harned, H. S.; Hamer, W. J. *J. Am. Chem. Soc.* **1935**, *57*, 27−35.

(35) Giauque, W. F.; Hornung, E. W.; Kunzler, J. E.; Rubin, T. R. *J. Am. Chem. Soc.* **1960**, *82*, 62−70.

(36) Hanson, D. R.; Ravishankara, A. R. *J. Phys. Chem.* **1993**, *97*, 12309−12319.

(37) Zhang, R.; Wooldridge, P. J.; Molina, M. J. *J. Phys. Chem.* **1993**, *97*, 8541−8548.

(38) Williams, L. R.; Golden, D. M. *Geophys. Res. Lett.* **1993**, *20*, 2227−2230.

(39) Elrod, M. J.; Koch, R. E.; Kim, J. E.; Molina, M. J. *Faraday Discuss.* **1995**, *100*, 269−278.

(40) Hanson, D. R. *J. Phys. Chem. A* **1998**, *102*, 4794−4807.